

Article

Comprehensive Evaluation of Lateral Performance of Innovative Post in Sand

Abdelrahman Abouzaid , Mohamed Hesham El Naggar *  and Osama Drbe

Department of Civil and Environmental Engineering, Western University, London, ON N6A 5B9, Canada; aabouza@uwo.ca (A.A.); odrbe@uwo.ca (O.D.)

* Correspondence: naggar@uwo.ca

Featured Application: The findings of this study hold significant implications for the field of geotechnical engineering, particularly in the design and construction of foundation systems for structures subjected to large lateral loads. The Innovative Post (IP) system presents a promising solution for enhancing the lateral load resistance of sound wall systems in layered cohesionless soils.

Abstract: Under environmental loads such as wind and earthquakes, piles are subjected to large lateral loads. A foundation system denoted Innovative Post (IP) that is composed of an H-pile shaft and one or two steel plates (paddles) welded to its flanges, has been developed to resist large lateral loads on sound wall systems. The present study evaluates the performance of IP installed in layered cohesionless soils through a comprehensive full-scale lateral load testing program and finite element (FE) analysis considering various pile and plate configurations. The developed FE model was validated employing the field test data and was then employed to conduct a parametric study to evaluate the performance of IP considering different paddles geometry (i.e., number of paddles, single or double, width, and length). The results demonstrated that adding the plates significantly increased the lateral capacity of H-piles. A positive relationship was identified between paddle's width and length and the load efficiency. Optimal parameter values for paddles are established based on the experimental and numerical results proposed.

Keywords: innovative post; paddled pile; lateral loading; sand; model tests; three-dimensional (3D) numerical analysis; finite element; design optimization



Citation: Abouzaid, A.; El Naggar, M.H.; Drbe, O. Comprehensive Evaluation of Lateral Performance of Innovative Post in Sand. *Appl. Sci.* **2024**, *14*, 2442. <https://doi.org/10.3390/app14062442>

Academic Editor: Francesca Pelosi

Received: 21 January 2024

Revised: 2 March 2024

Accepted: 4 March 2024

Published: 14 March 2024



Copyright: © 2024 by the authors. Licensee MDPI, Basel, Switzerland. This article is an open access article distributed under the terms and conditions of the Creative Commons Attribution (CC BY) license (<https://creativecommons.org/licenses/by/4.0/>).

1. Introduction

Steel H-piles find extensive application in providing support for structures like retaining walls, bridges, and sound walls. These constructions face lateral forces resulting from factors like retained soil and external elements such as wind and earthquakes. Consequently, substantial lateral loads and bending moments are imposed on their foundations. The repetitive occurrence of wind and earthquake forces can trigger significant and permanent lateral shifts in pile foundations, posing a potential risk of diminishing their lateral capacity [1,2]. This aspect holds particular significance in the design process, especially in scenarios involving substantial lateral loads and relatively lower vertical loads, as observed in the case of sound walls.

Numerous theoretical and practical investigations have been carried out to assess the lateral performance and capacity of individual piles. Matlock and Reese [3] presented comprehensive solutions for the lateral resistance of vertically loaded piles through non-dimensional analysis. Davisson [4] explored the impact of combined loads (both vertical and lateral) on pile lateral response. For calculating pile-head deflection resulting from lateral loads, Broms [5] introduced a simplified method grounded in subgrade modulus theory, assuming a linear increase in soil subgrade modulus with depth and linear elasticity of the soil. Matlock [6] and Reese et al. [7] introduced the concept of nonlinear (p-y) curves,

widely employed to determine lateral deflection, moment, and shear in piles subjected to lateral loads. This p-y curve is based on the subgrade reaction modulus approach developed by Winkler [8], replacing the soil around the pile with a series of closely spaced independent and elastic springs. Numerous research studies have examined the lateral capacity of innovative pile foundations, including those employing tapered piles and fin piles as explored in studies [9–11]. In a notable contribution, Peng et al. [12] conducted a comprehensive three-dimensional Finite Element Analysis specifically focusing on the lateral loading of fin piles.

Short-drilled shafts are commonly used to support laterally loaded sound walls because of their high lateral and uplift capacity. However, drilled shafts are considered unsustainable because their construction consumes a large amount of concrete [13]. In addition, the concrete curing process is time-consuming and may delay the construction schedule of sound walls, which affects the road work and causes traffic constrictions. Meanwhile, H-piles offer fast installation, reduced cost, eliminate the use of concrete, and are rendered immediately functional providing overall project cost and time savings. However, they lack the necessary lateral rigidity to fully sustain wind loads acting on superstructures, thus improvement is required to enhance their lateral rigidity and increase their lateral capacity. Existing approaches involve enhancing the surrounding soil, adjusting the dimensions of the pile, and employing battered piles.

A few studies investigated the effect of increasing the pile's cross-section or stiffening the pile by adding plates to a steel pile. Dührkap & Grabe [14] conducted laboratory small-scale tests simulating a prototype monopile 6 m in diameter and 25 m long embedded in sand. The result showed that the paddled pile is 65% stiffer than the plain pile. Lutenegger [15] conducted full-scale tension tests on driven finned piles. A total of four fins were welded to steel pipe piles embedded in an alluvial sandy silt supporting elevated solar panels. Abongo [16,17] carried out a small-scale experimental as well as numerical analysis to assess the lateral capacity of a steel pipe pile fitted with steel plates. The lateral capacity of the finned piles increased by 15% to 98% based on the number of fins and their orientation, and the lateral deflection decreased by over 65% compared to monopiles. In addition, the pile length required to achieve the same lateral performance was reduced by as much as 40%. Pei & Qiu [17] conducted a parametric study using finite element (FE) analysis to evaluate the effectiveness of steel fin pipe foundations (SFPFs) in resisting lateral load and reported that SFPFs demonstrated significantly higher lateral resistance than unfinned piles.

Peng et al. [12] mentioned that the predominant emphasis in existing research on finned piles has been directed toward enhancing the lateral load capacity of unfinned pile foundations, specifically those utilized for offshore wind turbines, typically characterized as pipe piles. It's worth noting that for various infrastructure projects such as sound walls, other types of piles like H-piles are often considered more suitable and practical. Mroz [13] conducted a full-scale monotonic and cyclic lateral loading on the IP (plate-modified H-pile) in clay. Plates with 950 mm length, 420 mm width and, 9 mm thickness were welded to the piles to form the IP. A total of 14 steel W8 × 24 (W200 × 36) H-piles were tested (4 H-piles, 8 single-paddled, and 2 double-paddled), with an embedded length of 3.5 m and with 1.35 m stickup. Two drilled shafts were also constructed and tested, and their response with that of the IPs. In addition, a limited parametric study was conducted using Lpile v2019 software. The study concluded that single-paddled piles have 22% higher capacity than the unpaddled pile. To better understand the behavior of the paddled H-piles in clayey soil, Abouzaid and El Nagar [18] conducted a three-dimensional finite element analysis using PLAXIS 3D v20 to investigate the effect of soil consistency, paddle's length, and paddle's width on the lateral capacity of the PHPs. Mroz [19] tested PHPs in clay, however, the performance of the double paddle pile was affected by the installation disturbance (the operator swayed the piles laterally), and the performance of the IP system in sand was not evaluated.

This work addresses the market's need for an enhanced foundation system tested in sandy soil. This study presents the results of a full-scale field-testing program that was conducted to investigate the lateral performance and capacity of double-paddled steel H-piles embedded in sand. In addition, a finite element model (FEM) was established using FE software PLAXIS 3D to simulate the test piles and was validated employing the field test results. The validated FE model was then used to conduct a parametric study to evaluate the performance of single-paddled and double-paddled IP systems under different soil conditions. In addition, the influence of the plate's width and length on the pile's lateral capacity was assessed. Subsequently, the behavior of the IP under lateral loading and its influence on surrounding soil are discussed. The outcomes of this study have the potential to establish design protocols for PHPs, and offer valuable insights for advancing engineering methodologies pertaining to foundation systems under lateral loading conditions.

2. Site Investigation Program

The IP piles were installed at a test site on 640 Waydonm Drive, in Ayr, Ontario. Four boreholes BH-1, BH-2, BH-3, and BH-4 were drilled within the site. Figure 1 illustrates the site layout and locations of the boreholes and the test areas. A Diedrich D-50 track-mounted drill rig equipped with an automatic hammer and continuous flight hollow stem augers was used to advance the boreholes. Soil samples were retrieved from each borehole, using hollow stem augers. In addition, standard penetration tests (SPT) were conducted utilizing standard split spoon equipment. Observations of groundwater were taken in the boreholes during and after drilling. Soil laboratory testing program was conducted, which involved determining the natural moisture content of the recovered split spoon samples, twenty particle size distribution assessments (five samples per borehole) on representative samples of the predominant subgrade soil types.

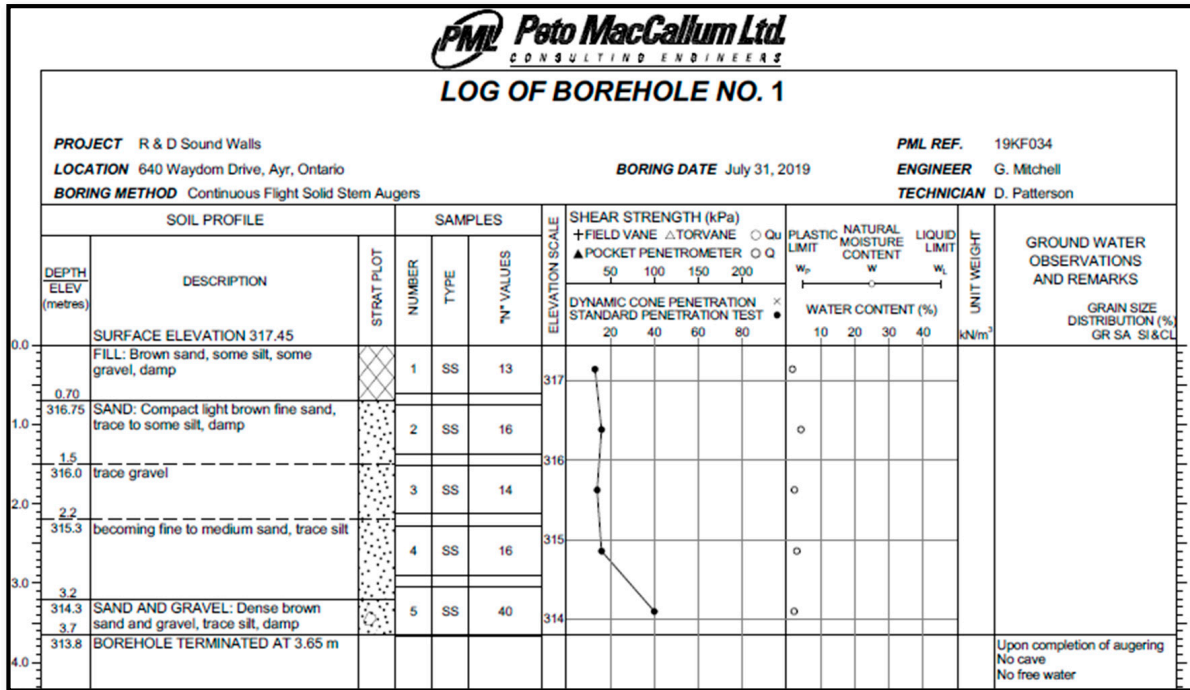


Figure 1. Atlantic Industries Ltd. (AIL) facility layout and locations of boreholes.

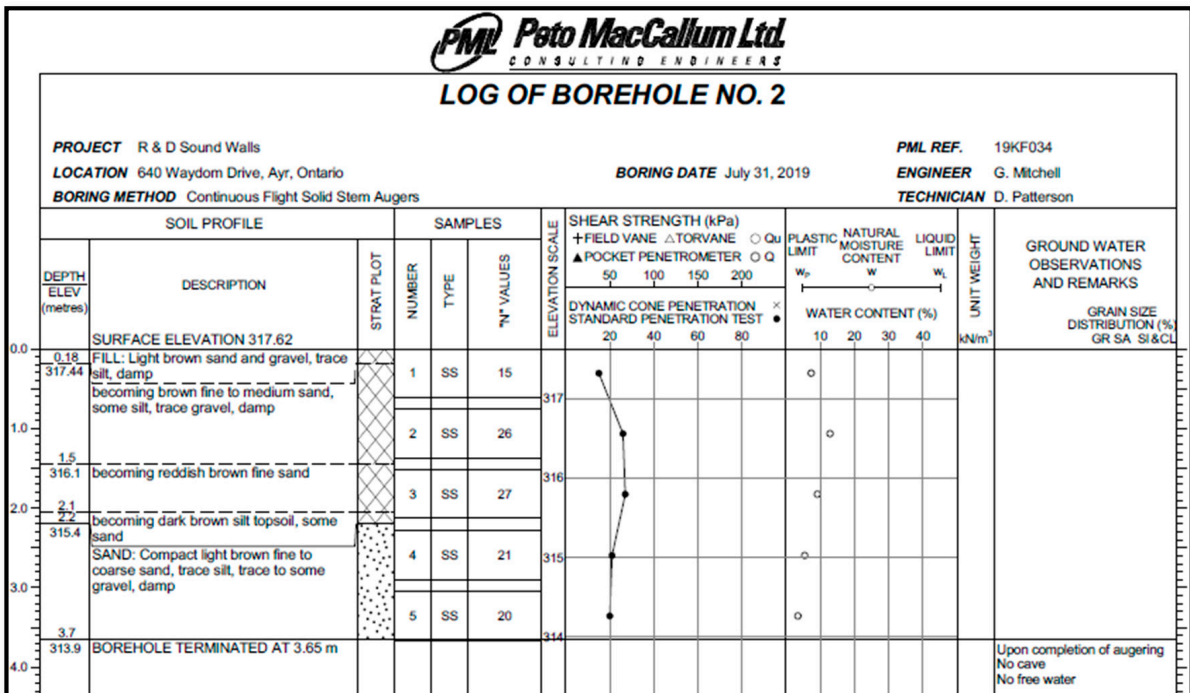
Soil Profile and Soil Properties

As shown in Figure 2a the soil profile in BH-1 comprises a layer of fill 0.6–0.7 m thick made of sand with some silt and gravel, overlaying a layer of fine sand 2.3 m thick, which lies over a layer of sand and gravel with trace silt. A layer of dense sand and gravel appears

below depth 3.2 m with an SPT value of 40 blows. The water content ranged between 2 to 5% with an average of 3.4%. The soil color changed from brown to light brown at 700 mm below the ground surface as the water content increased. BH-2, shown in Figure 2b, was terminated at a depth of 3.7 m. It indicates a layer fill 2.4 m thick of fine sand with silt underlain by a layer of brown fine to coarse sand with some to trace gravel and trace silt that extends to 3.7 m (end of borehole) below ground surface.



(a)



(b)

Figure 2. Borehole logs: (a) borehole 1; (b) borehole 2.

The mechanical and strength parameters of the sand were evaluated employing empirical correlations with SPT N value. Because empirical correlations give a wide range of values for the same N value, various correlations available in the literature were considered. Using a trial-and-error methodology, and comparing load-displacement data from the field and the FE model allowed the selection of the correlations that best represented the soil properties at site. The soil unit weight was determined using the Kedzi [20] relationship. The empirical correlation of the secant modulus, $E_s = 6 \times N$ proposed by Bowles [21], was used to estimate the sand elastic modulus. Bowles's correlations for all types of sand were found to be representative for loose to medium normally consolidated (NC) sands. Whereas for medium to dense normally consolidated sand, the correlations of Bowles for normally consolidated sand, provides a good estimation of secant modulus. Kumar et al. [22] suggested correlations that give a good estimation of Poisson's ratio. Kulhawy et al. [20,23] proposed a correlation that was used to obtain the friction angle. Table 1 summarizes the established soil parameters and the used empirical correlation.

Table 1. Summary of the established soil parameters.

Parameter	Unit		BH.1			BH.2		
Depth	m		0–0.7	0.7–3.2	3.2–3.65	0–0.3	0.3–2.2	2.2–3.65
N	blows		13	15	40	15	26	21
N_{60}			13	15	40	15	26	21
$(N_1)_{60}$			13	18	45	15	31	25
Source								
γ	KN/m ³	[20]	18.5	18	21	18.5	18.25	18
ϕ'	(°)	$\phi' = 27.5 + 9.2 \log(N_1)_{60}$ [23]	38	39	43	38	41	40
E_s	MPa	$E_s = 6000 N$ [21]	78	90	240	90	156	126
μ		$\mu = 0.2 + 0.01 N$ $0 < N < 20$ $\mu = 0.2 + 0.005 N$ $20 < N > 50$ [22]	0.33	0.35	0.4	0.35	0.33	0.31

3. Innovative Post Pile (IP)

Full-scale pile load tests were conducted in two groups (Group 1 in 2019 and Group 2 in 2020) on four configurations of the IP to assess its lateral capacity and performance characteristics. Group 1 involved two-paddled IP piles that were manufactured by welding paddle-shaped steel plates to both flanges of an H-pile with W150-37.1 section. The plates were shifted 20.0 cm from the pile head to allow connecting the load cell. The H-pile cross-section was 162 mm deep, 154 mm wide and the web and flange thicknesses were 8.1 mm and 11.6 mm, respectively. Two different configurations of the paddles were utilized and the resulting two-paddled pile configurations were named: S10, S12, and S16. The configuration S10 and S16 refer to the pile with a plate 500 mm wide and 12.5 mm thick, while the S12 configuration involved 400×12.5 mm plates. The paddle configurations were 1.7 m, 2.2 m, and 2.0 m long for S10, S16, and S12, respectively, without considering the length of the 450 stringers at the end of the plate. The piles were installed close to BH-1. Group 2 involved testing the S20 IP configuration, which were manufactured by attaching the paddles to the flanges of the posts by means of two columns of "C"-shaped steel clips (instead of welding). Each clip was 200 mm \times 100 mm. All clips were bent at a 45-degree angle and vertically spaced at 600 mm, and 700 mm c/c from the first and second respectively. The horizontal distance between the edges of the two columns of clips was 50 mm. In Group 2 piles, there was no space between the paddles and the base plate. To attach loading equipment, two vertically slotted holes were pre-drilled on the paddles and flanges of the W-section. The full-scale posts were fully embedded into the ground, 20 cm of soil was excavated from one of the sides of the flanges to attach the equipment. S20 pile tests were carried out in the year 2020 and close to BH-2. Figures 3 and 4 provide a

summary the different configurations of the tested innovative posts, and a typical layout of the tested piles.

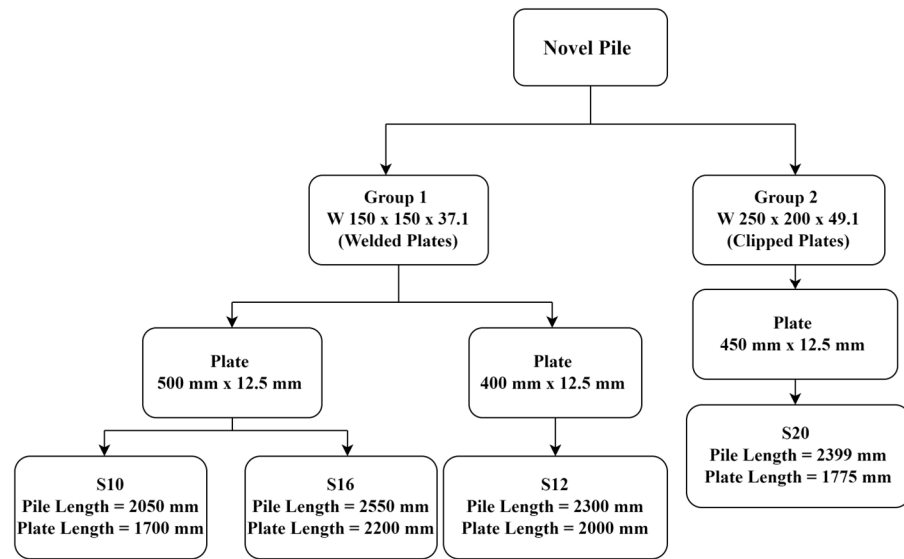


Figure 3. Summary diagram for the various tested innovative posts.

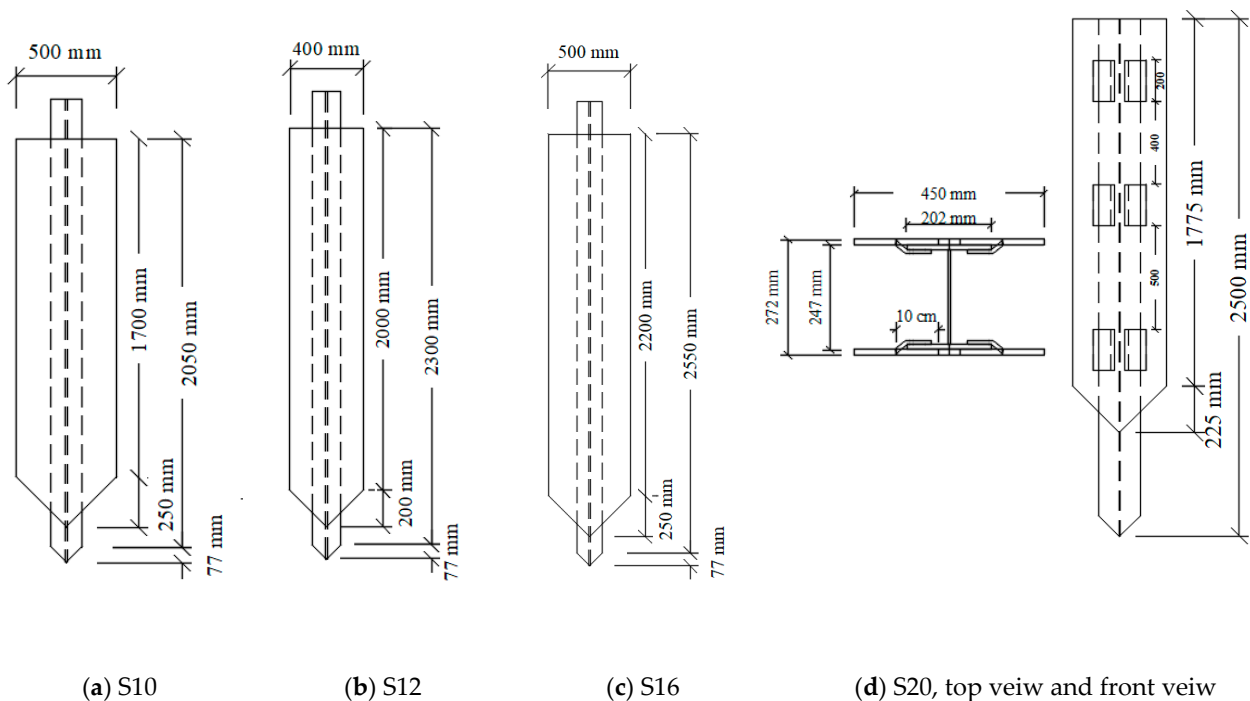


Figure 4. Pile designation and configurations and its cross-sectional dimensions for Group 1 (a–c), and Group 2 (d).

4. Load Testing Program

4.1. Test Setup and Pile Installation

The monotonic lateral load test was carried out in accordance with ASTM standard D3966M-07 [24]. A 500 kN load cell was placed between the hydraulic jack and the post to record the load. In Group 1 tests, the hydraulic jack was pushing against the test innovative post and concrete blocks. In Group 2 tests, the hydraulic jack was pushing against the test innovative post and another post. Two displacement gauges (LVDTs) were placed behind the post, close to the edges of the pile head, to measure the lateral displacements of the innovative posts.

During the test, if the hydraulic jack was fully extended without reaching the target load, it would be retracted and extra spacer beams would be placed, and the loading test would be repeated. In Group 2 tests, two innovative posts were tested simultaneously, thus the load cell and the hydraulic jack were positioned between both piles. Therefore, the rigid resistance system was unnecessary, and two steel rods were employed to ensure that there is no gap between the test instruments and the flanges of the two posts. The steel struts were connected to the plates directly; thus, the loading plates were not used. All components were leveled before conducting the test. Figure 5 demonstrates Group 1 and Group 2 test setup and pile instrumentation.

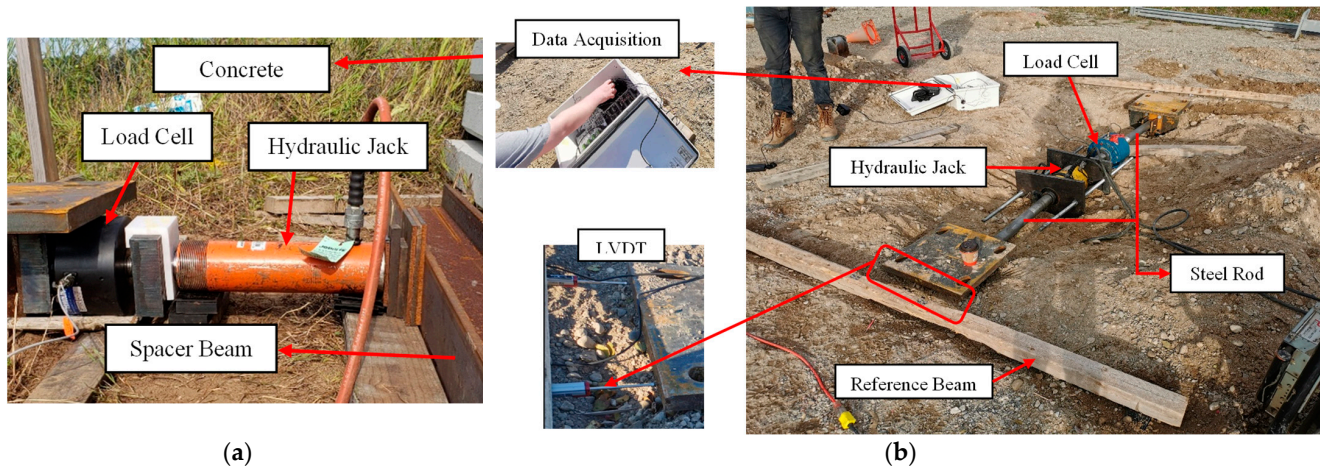


Figure 5. Test setup and pile instrumentation: (a) Group 1 tests; (b) Group 2 tests.

4.2. Lateral Monotonic Test Result

In Group 1, a series of 5 double-paddled innovative posts were tested under lateral load control. The data for load-displacement behavior was recorded and compared. The lateral load test was conducted on a single specimen of S12 and S10, as well as on three distinct specimens of S16. A total of four double-paddled innovative posts, with clipped plates, were tested in 2020 (Group 2 tests).

4.3. Load Displacement Curve

Two groups of posts (Group 1, and Group 2) were tested. The first set was made up of a w-section pile with two welded plates at the flanges, whereas the plates in the second group were attached to the pile with clips. The paddled piles were loaded along the weak axis (i.e., axis with the lower moment of inertia). Figure 6 depicts the horizontal load-displacement responses of Group 1 posts, the ultimate capacity of S10, S12, and S16 established from the load tests were 95 kN, 82 kN, and 125 kN, respectively (considering an average value for S16 tests excluding the third test).

The residual displacement after unloading for the pile was approximately 4.8 mm, 8 mm, and 4 mm for innovative posts S10, S12, and S16, respectively. In other words, the piles recovered up to 61.5%, 57.4%, and 75.0% of the displacement throughout the unloading process. It should be noted that the third test for the S16 pile deviated from the other two tests, showing a much lower lateral resistance than the other two tests. The softer behavior and lower capacity are attributed to high soil disturbance during the installation (based on observations during installation). In Group 2 tests, the 450 stringers at the end of the paddle were bent during the installation of the fourth specimen of the S20 pile. Therefore, the soil around the pile was disturbed, and the pile exhibited significant lateral displacement, as shown in Figure 7. The installation method (vibratory driving in dense sand) and installation process of the clipped piles (Group 2 piles) caused disturbance to the adjacent soil, this disturbance is mainly related to installation difficulty (i.e., which required shaking the pile, lifting and reinstalling it), and the “C”-shaped steel clips which

most likely increased soil disturbance. According to the field testing results, the ultimate lateral capacity of the S20 posts ranged from 212 kN to 196 kN, with an average of 204 kN corresponding to lateral displacements of 24.5 mm, 26 mm, and 23 mm, respectively. The recorded residual displacement has an average value of 11 mm.

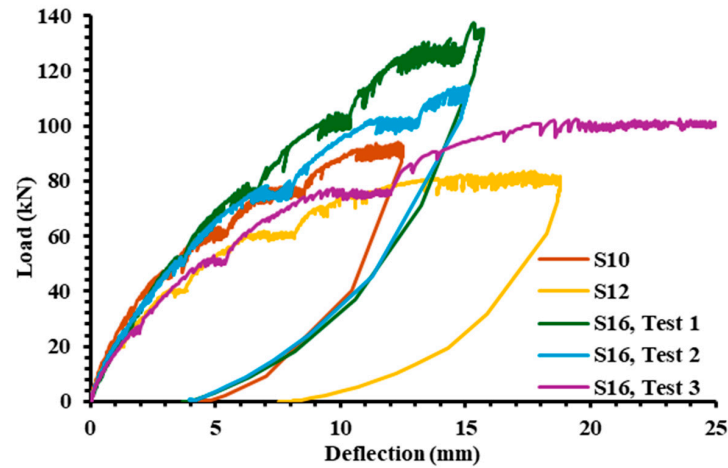


Figure 6. Load-displacement curves obtained from pile load tests, for Group 1 tests: S10, S12, and S16.

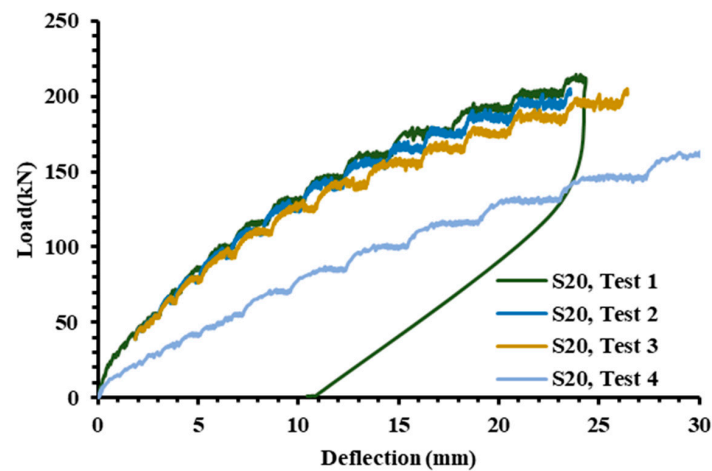


Figure 7. Load-displacement curves obtained from the pile load tests, for Group 2 tests: S20 innovative post.

To evaluate the performance of the FEM 3D models compared to field data, the error was calculated considering various failure criteria based on pile head lateral displacements: 6.25 mm by McNulty [25], 13 mm by Walker and Cox [26].

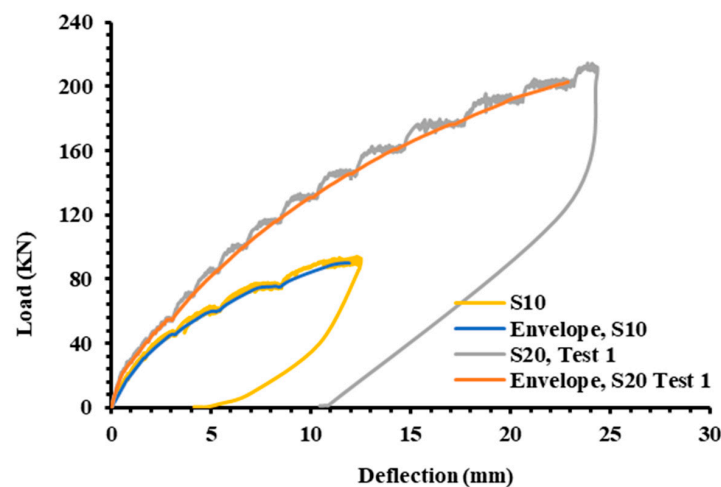
$$\text{Error (\%)} = \text{Load} \left(\frac{\text{Field} - \text{FEM}}{\text{Field}} \right) \times 100 \quad (1)$$

Table 2 compares the pile lateral capacities considering the different lateral failure criteria, derived from field test data, with those obtained from the 3D Finite element analysis. It is noted that, for S20, as the tolerance value increases, the error percentage reduces dramatically. The deviation of the FEM model from the field results at lower failure criteria can be attributed to the creation of the gap between the soil and the pile due to installation practice. Overall, the low error percentages observed demonstrate that the FEM scheme used herein is suitable for replicating the response of the PHPs and hence PLAXIS 3D can be used as a reliable tool for their design.

Table 2. Comparison of lateral load capacity different design methods.

Specimen		Failure Criteria		Difference (KN)		True Error (%)	
		6.25 (mm)	13 (mm)				
S10	PLAXIS Field	61.55 70.614	79.54 -	-9.064	-	-12.84%	-
S12	PLAXIS Field	64.53 64.55	87.87 79.87	-0.02	8	-0.03%	10.02%
S16	PLAXIS	78.72	111.76				
S16 (1st)	Field	75.71	128.24	3.01	-16.48	-3.98%	12.85%
S16 (2nd)	Field	73.84	100.99	4.88	10.77	-6.61%	-10.66%
S20	PLAXIS	121.3	165.14				
S20 (1st)	Field	100.22	161.03	21.08	4.11	-21.03%	-2.55%
S20 (2nd)	Field	95.4	153.6	25.9	11.54	-27.15%	-7.51%

The anticipated load-displacement behavior of a pile under lateral load may be segmented into three phases. The first segment represents linear behaviour. This is followed by a nonlinear response segment that tends toward plasticity. The last stage is characterized by full slippage along the side of the pile's body and complete plasticity of the bearing soil manifested by another linear segment. Drbe and El Naggar [27] and Abouzaid and El Naggar [18] reported the same behavior for laterally loaded micropiles and PHPs in clayey, respectively. Guo et al. [28] observed sand heaving concurrently with gap opening during the second phase. Figure 8 illustrates the typical envelope behavior of the two posts, showing the initial linear response, followed by the nonlinear response and then a straight line.

**Figure 8.** Load-displacement curve and envelope load-displacement curve for S10 and S20 posts (test 1).

The S20 posts displayed a generally more rigid response than the Group 1 piles, as well as a significantly higher ultimate capacity, due to the notable difference in the moment of inertia around the weaker axis between S10, S16, S12, and S20 posts (i.e., 1.18×10^{-4} , 0.98×10^{-4} , and 2.59×10^{-4} , respectively). This may also explain why S12 displayed less displacement than S10.

Failure Mechanism

The pile ultimate lateral capacity depends on the characteristics of the surrounding soil and the pile material and cross-section and length. Long innovative posts are considered flexible piles, and short innovative posts are considered rigid piles, primarily based on their rigidity slenderness and relative rigidity compared to surrounding soil. The pile slenderness ratio, L/D , indicates the pile type and its potential mode of failure. The

ultimate lateral capacity of long piles is dictated by its flexural stiffness. In this case, as the applied lateral load increases, the maximum bending moment that develops at the pile cross-section increases until it reaches the yield moment of the pile. The short pile lateral resistance is primarily influenced by the soil strength. This resistance corresponds to the applied lateral load that develops yield strain within the soil mass in front of the pile shaft. The failure of a short pile with fixed-head condition occurs due to lateral displacement, while failure of a short pile with free head condition is a consequence of the pile rotation which leads to passive soil resistance with high strains on the front side of the pile upper portion and behind the lower portion of the pile (below the point of rotation).

Pile stiffness assessment can be conducted by considering the ratio of embedded length to diameter, denoted as L/D . A pile with an L/D ratio less than 6 typically exhibits behavior characteristic of a short pile, while one with an L/D ratio greater than 10 is more inclined to behave like a long pile, as indicated by previous studies [29] Kasch et al. [30] established a threshold for flexible piles, defining them with L/D values exceeding 20. Evaluation of pile rigidity may entail determining the pile flexibility factor, denoted as K_r , as presented by Poulos and Davis [31].

$$K_r = \frac{E_p I_p}{E_s L_p^4} \quad (2)$$

where E_p and E_s are Young's modulus of the pile and soil, I_p and L_p are the moment of inertia of and embedded length of the pile. It is anticipated that short piles will have $K_r > 0.01$, while flexible piles will have $K_r \leq 10^{-5}$.

The allowable design load for sound walls is usually governed by the serviceability limit state rather than the ultimate limit state. Hence, the experience-based lateral serviceability standards for piles are established. The capacity of piles to resist lateral forces is characterized by the load applied at the pile head, corresponding to a specific lateral deflection of the pile head. Consequently, this discussion incorporates various failure criteria grounded in pile head lateral displacements. Table 3 presents different lateral failure criteria and the associated pile lateral capacities derived from field test data aligned with these criteria. As expected, the lateral capacity increases as the lateral deflection tolerance increases. It is also noted that there is some minor variability of the lateral capacity of the piles that have the same configuration. Finally, it is obvious that the lateral capacity increases as the pile cross-section and the plate size increase.

Table 3. Ultimate lateral capacity for the innovative posts.

Reference	Criteria Load at	Ultimate Design Lateral Capacity, (KN)						
		S10	S12	S16		S20		
				Test 1	Test 2	Test 1	Test 2	Test 3
[25]	6.25 mm	71	60	77	73	100	95	96
[26]	13.0 mm	87	80	128	100	162	153	140
[32]	25.0 mm	-	-	-	-	-	-	193

5. Numerical Investigations

The three-dimensional (3D) process involved in resisting the lateral forces include passive lateral soil resistance along the leading face of the pile, and shearing along the toe of the shaft and around its perimeter. Moreover, axial forces can influence lateral behavior. This 3D complex behaviour necessitates a sophisticated 3D analysis [33]. Therefore, finite element (FE) modeling is used for the design of structures exposed to complex loading systems [34], and to account for the non-linearity of the soil-pile system. The FE approach can consider the pile-soil system as a single composite continuum in which a direct pile-soil-pile interaction is considered [35,36]. The three-dimensional finite element program

Plaxis-3D was employed to establish 3D finite element models that were calibrated using the results of both Group 1 and Group 2 pile load tests.

5.1. 3D Finite Element Modeling

The numerical simulation was conducted using the three-dimensional finite element software PLAXIS 3D Foundation. The geometric model simulated the exact geometry of the tested innovative posts and their material properties, the soil medium around the piles and its properties as well as the applied loading conditions. The local soil stratigraphy was defined using the information from the boreholes. The pile volume used in the numerical model replicated the actual geometry of the test piles. After defining the entire geometry model and assigning initial properties to all geometry components, the finite element mesh was generated. The 10-node tetrahedral elements were employed to discretize the soil domain, which enabled displacement interpolation of the second order, to accurately simulate the elements deformation and capture the geometric curvatures.

5.1.1. Defining Material Parameters

A set of mathematical equations that describe the relationship between stress (effective stress) and strain rate characterize the material model. Frequently, material models are defined so that infinitesimal stress or stress rates are associated with microscopic strain or strain rates [37].

Two types of materials were used in this study: steel to model the innovative post; and soil to model the different soil layers. The linear elastic model (LE) was used to simulate the behavior of the pile, while the linear elastic perfectly plastic (Mohr–Coulomb, MC) model was used to simulate the soil. The LE is used for elastic–perfectly plastic material. Its formation is based on Hooke’s law of isotropic linear elasticity and is mainly used for stiff structures in soil. The LE model is defined mainly by Young’s modulus (E), and Poisson’s ratio (ν). The LE model is suitable for simulating the structure material which has much higher strength properties than the soil (i.e., concrete wall, and Steel piles). Chik et al. [38] and Deendayal et al. [39] presented a 3D FE analysis to simulate a lateral load test utilizing PLAXIS 3D with a Mohr–Coulomb elastoplastic model for the soil. The MC model’s linear elastic component is based on Hooke’s law of isotropic elasticity. In contrast, the perfect plastic region is based on the MC failure criterion, which is formulated in a non-associated plasticity framework.

Table 4 shows the different stiffness and strength parameters that are used for both models. Since the soil consisted of sand layers, the drainage type was set to “Drained” to account for the high porosity of the sandy soil. Thus, effective strength and stiffness soil parameters were used. The soil parameters were derived from the SPT N values. Young’s modulus, E , corresponded to the loading-reloading modulus of elasticity, E_{ur} , in the Mohr–Coulomb model, where $E_{ur} = 2-6 E_s$, where E_s is the secant Young’s modulus [40]. As the soil profile comprised sand layers, the user input Young’s modulus, E , in the model was set equal to $3 E_s$. For Group 2 tests, weaker soil layers have been defined around the pile with Young’s modulus equal to E_s , to account for soil disturbance due to driving. The zone of disturbance ranges from 3 to 5.5 times the pile diameter away from the pile shaft and 3 to 5 times the pile diameter below the pile toe [5].

Since the friction between the soil and pile at the pile shaft and pile tip is less than the internal friction of soil, the interface element was applied in this study to account for the interface resistance. The interface element is a zone with the same material properties as the adjacent soil and a virtual thickness. During the slipping stage, decreased values for stiffness parameters will be employed, and the value of strength parameters will decrease by a strength reduction factor ($R_{inter} < 1$) [33]. As an acceptable assumption, a strength reduction factor of $0.65 \times \tan(\Phi)$ was applied to the R_{inter} to simulate the steel-soil interface [12,17,41,42].

Table 4. Material properties for PLAXIS 3D model.

Parameters		Pile	Group 1 Tests			Group 2 Tests			
			layer 1	Layer 2	Layer 3	Layer 1	Layer 2	Layer 3	
General	Unit	Reference							
Material Model			Linear elastic			MC			
Drainage type			Non-porous			Drained			
γ_{sat}	(KN/m ³)	[20]	78.5	18.5	18	21	18.5	18.25	18
γ_{unsat}			-	19	19	20.5	19	19.5	20.5
Soil Parameter									
$E = 3E_s$	(MPa)	[21]	2×10^5	240	270	360	270	450	360
ν	-	[22]	0.3	0.33	0.35	0.4	0.35	0.33	0.31
Φ	Degree	[23]	-	38	39	43	38	41	40
$\Psi = (\Phi - 30)$		[37]	-	8	9	13	8	11	10

5.1.2. Boundary Conditions and Mesh Refinement

To avoid the effect of boundary in the numerical model on the soil-structure behavior, the model boundaries were placed at a distance more than 10 times the width (B) of the innovative post. The size of the FE model was 5 m by 5 m, for Group 1 and 2 tests. A convergency study was carried out for varied sizes of mesh and coarseness factors. The medium element distribution meshes size and coarseness factors of 0.5, 0.25, and 0.1 resulted in a good agreement with the experimental result. Figure 9 shows the typical 3D FE mesh used to assess the innovative posts subjected to lateral loading. The surface load feature in PLAXIS 3D was utilized to simulate the field loading procedure. The load given in (KN/m²) was applied in the horizontal Y-direction. The load surface had the same area as the steel struts, which were connected to the tested plate, described in Section 4.1.

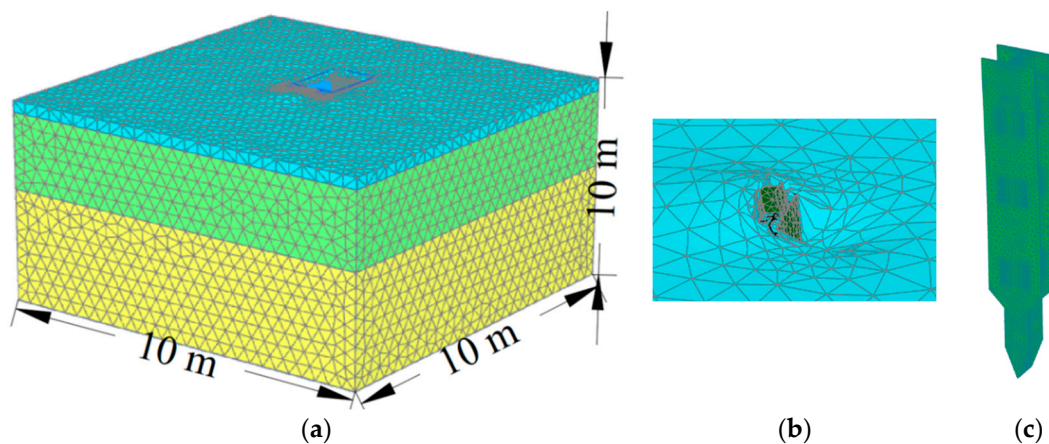


Figure 9. FE model: (a) 3D mesh; (b) soil movement around pile head; and (c) pile geometry.

The number of nodes and elements for different models are presented in Table 5. Due to the relatively small geometry of the clips, the models for the S20 had a minimum element size of 0.01×10^{-3} , hence the models had significantly more nodes and elements than the other models.

Table 5. Number of nodes and elements for various mesh models.

Model	S10		S12		S16		S20	
	DP	SP	DP	SP	DP	SP	DP	SP
Number of nodes	90,049	83,117	88,679	86,999	92,737	94,917	407,471	408,947
Number of elements	57,562	54,073	56,716	56,707	59,928	60,033	238,117	238,502

5.2. Calibration of PLAXIS 3D Numerical Models with Field Load Tests

The field tests of the innovative post-S16 were utilized to calibrate the Group 1 tests model. Figure 10 demonstrates a satisfactory agreement between the computed and measured data. The model was then validated by comparing its response to field data of innovative S10 and S12 posts with varying embedded length and/or plate width compared to S16. A similar approach was used to calibrate the FE model of the S20 innovative post. The S20 model was calibrated with the result of the first test and validated by the other two tests.

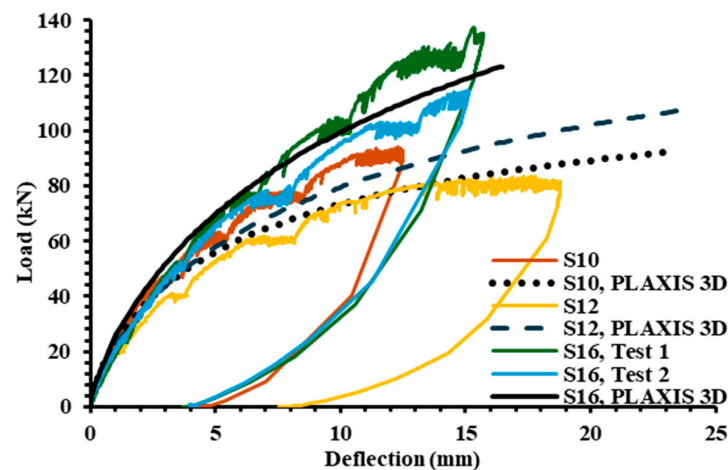


Figure 10. Numerical and experimental load-displacement curves for innovative posts S10, S12, and S16.

Figure 11 demonstrates that the numerical model results agree well with the field findings, especially in the initial linear region. This indicates accurate simulation of the soil elastic behavior. Meanwhile, for higher load range (e.g., 25 kN to 175 kN), the FEM results suggest a slightly more rigid response compared to the field data. Overall, there is a general agreement between the numerical results and the observed response in the field tests up to the maximum applied lateral load.

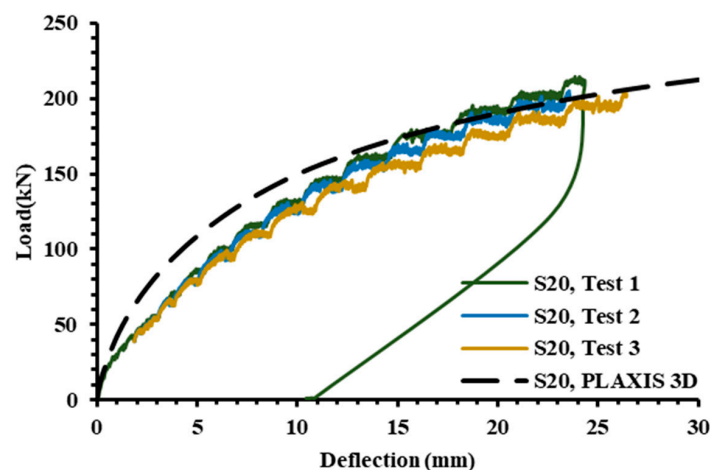


Figure 11. Numerical and experimental load-displacement curves for innovative post S20.

6. Parametric Study

The performance of the paddled H-pile with a single plate welded in the opposite direction of the load (single-paddled pile, SP) is compared to the performance of double-paddled piles, DP. In addition, the influence of plate width and length on the single-paddled and the double-paddled innovative post lateral capacity is evaluated. Furthermore, the effect of plates on the surrounding soil is investigated. This study considered S16

dimensions of 2200 mm × 500 mm × 12.5 mm. The pile is embedded in sandy soil with the properties of the second layer in Table 4.

6.1. Performance of Single-Paddled Posts

A single-paddled pile is anticipated to have a lower lateral resistance than double-paddled piles (i.e., the system that was tested in the field). The lower resistance is attributed to three factors: a lower moment of inertia, a smaller soil-pile interface area and the absence of soil confinement between the two plates. For the different innovative post configurations considered (i.e., S10, S12, S16, and S20), similar pile configurations with only one plate are considered in the analysis. Since wind loads can act on the paddled flange (Case 1) or on the opposite flange (Case 2), a study is conducted first to determine the worst-case scenario for the location of the paddle relative to the load direction. As demonstrated in Figure 12, Case 2 exhibited lower lateral resistance and, therefore, it is considered for the ensuing parametric study.

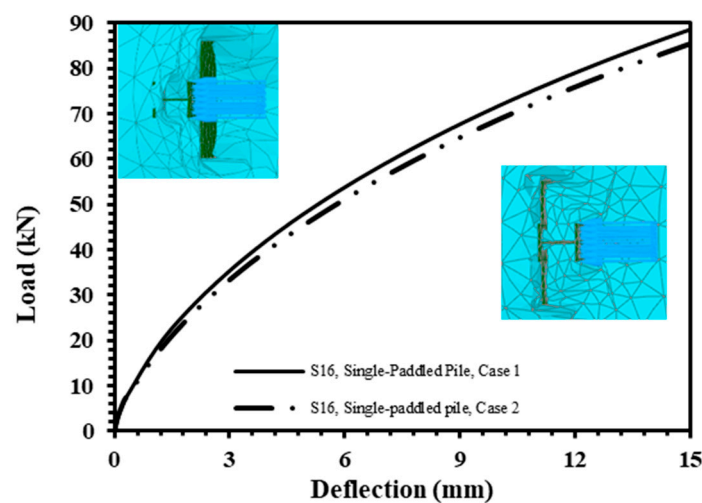


Figure 12. Comparison of load-displacement curves considering different load directions.

The validated model was used in the analysis and the paddle was considered attached to the flange opposite to loading direction (i.e., Case 2). The pile lateral capacity was established based on pile-head lateral displacement failure criterion provided by Walker and Cox [26], i.e., the lateral capacity is the load that caused a pile head lateral displacement of 13 mm. Table 6 compares the lateral load capacity of the single-paddle (SP) and double-paddle (DP) piles.

Table 6. Comparison of lateral load capacity of single- and double-paddled posts.

Pile Type		Load at 13 mm (kN)
S10	DP	79
	SP	68
S12	DP	88
	SP	72
S16	DP	112
	SP	80
S20	DP	165
	SP	145

As expected, DP posts have higher lateral load capacity owing to the additional stiffness and resistance related to the second plate. It is also noted from Table 6 that S16 exhibits the highest percentage increase in pile capacity (i.e., 40%) due to the second plate. This increase in capacity is a result of the plate size of S16 ($L = 2.325$ m and $W_p = 0.5$ m),

which significantly increases the pile-soil interface area and passive resistance. Compared to the other post configurations, the lateral capacity of the double-paddled S20 improved only marginally, 13.7%, which can be attributed to the small ratio of plate-to-pile width: $W_p/W_f = 450/202 = 2.23$.

6.2. Effect of Plate Width

In this section, we examine the influence of plate width on the lateral capacity of SP and DP posts. The plate width was systematically altered in 25% increments, ranging from 0.25 to 2.25 times the initial width of S16. Figure 13 depicts an incremental increase in the pile capacity by 57%, 29%, and 21% for W_p/W_f equal to 1.6, 2.4, and 3.1, respectively, indicating that at low width of plate-to-pile ratio the size of the plate significantly affects the lateral capacity of the double-paddled pile.

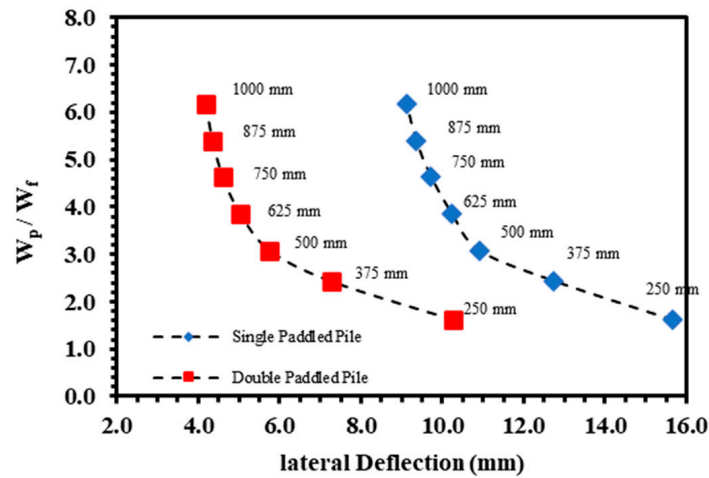


Figure 13. Relationship between lateral deflection and plate width normalized by pile width.

In contrast, the single-paddled pile’s capacity experiences a relatively minor impact from an increase in plate width, showing a 35% capacity increase for a plate width of 250 mm and a 19% increase for a width of 375 mm. Notably, it becomes evident that as the plate-pile flange width ratio rises, the influence of the plate width on displacement diminishes. Figure 11 further illustrates that when the plate is four times the width of the pile’s flange in a double-paddled pile system and three times the width in a single-paddled pile system, the effect of plate width on lateral displacement becomes negligible. Additionally, the lateral deflection of double-paddled piles consistently measures approximately 5 mm, indicating a stiffness 25% to 30% greater than that of a single-paddled pile across all W_p/W_f ratios.

The effectiveness of the innovative posts was also assessed through a stiffness efficiency parameter, denoted as η_S . This parameter is defined as the enhancement in the lateral stiffness of the pile under a specific lateral load when compared to an equivalent plain pile.

$$\eta_S = \frac{S_{PP} - S_P}{S_P} \tag{3}$$

where S_{pp} and S_P are the lateral stiffness corresponding to the lateral head displacement at a given load for paddled pile and plain pile, respectively.

Figure 14 shows the stiffness efficiency curve, which indicates that the variation of the paddled H-pile lateral stiffness with the plate width. It is clear that η_S increases as the plate width increases. This indicates that stiffening the pile with one or two plates substantially enhances the stiffness of the foundation system and can provide from 121% to 318% more rigidity (with a plate width of 500 mm) than the corresponding plain pile. As expected, the double-paddled piles demonstrate greater stiffness than single-paddled piles for the same plate width. Figures 13 and 14 show that a double-paddled pile can provide up to more

than 100% stiffness than the corresponding single-paddled pile. This significant increase is related to the increase in the geometry of the innovative post and due to the confined soil between the two plates. However, it is anticipated that the double plate would be more expensive. Hence, single-paddled posts may have an economic advantage.

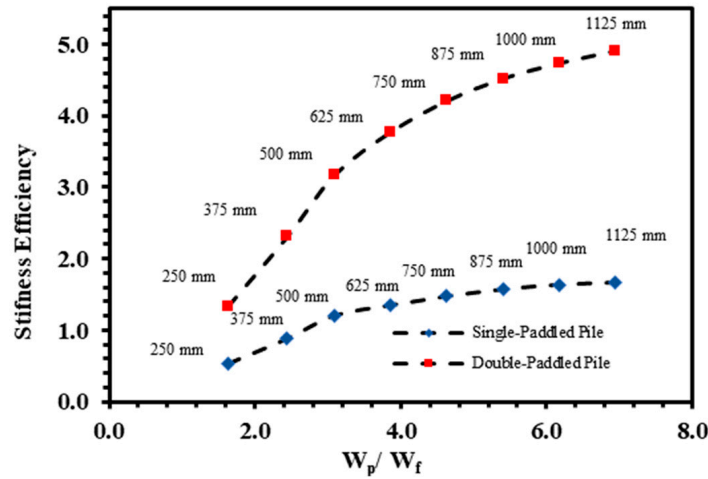


Figure 14. Stiffness efficiency for various W_p/W_f values.

Figure 15 illustrates the variation in the maximum bending moment along the pile shaft. The outcomes reveal a reduction in the maximum bending moment due to the presence of plates, with a noticeable decrease as the plate width increases. However, for W_p/W_f values equal to or exceeding 5.4, the reduction in bending moment becomes negligible. The plates play a role in resisting a portion of the bending moment, thereby reducing the overall bending moment in the H-pile. Additionally, it is observed that the depth of the maximum bending moment decreases with an increase in plate width. These observations align with the findings reported by Abouzaid and El Naggar [18], Abongo [16] and Pei and Qiu [17].

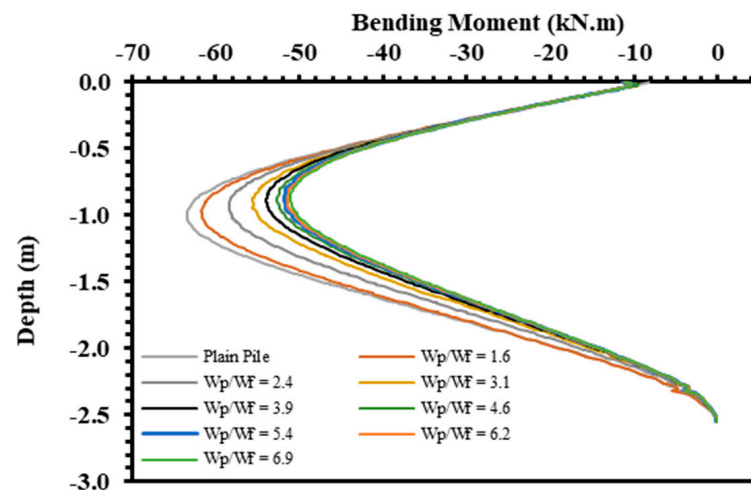


Figure 15. Bending moment versus depth of double-paddled piles with various plate width.

6.3. Effect of Plate Length

The effect of plate length on the lateral response of the innovative post is assessed in this section. Figure 16 displays the effect of plate length normalized by its width, L/W_p , on the lateral capacity of the innovative post for two cases: plates are connected to an H-pile with a fixed embedded length of 3.5 m; and a post with identical pile and plate lengths.

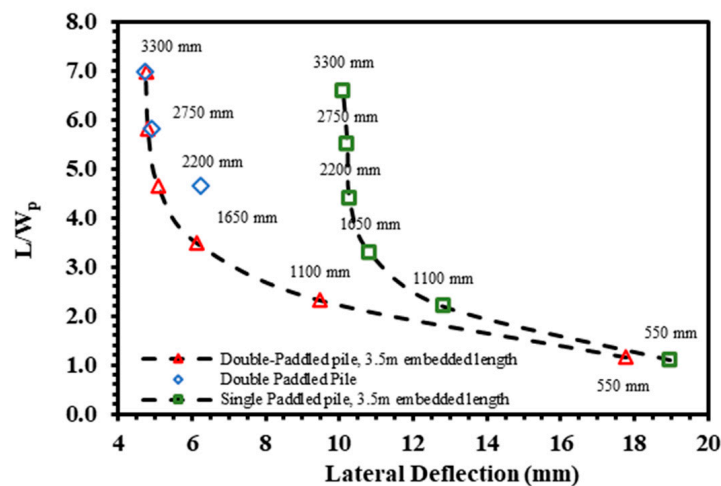


Figure 16. Relationship between lateral deflection and the length of the plate normalized by the width of the pile.

For a fixed-length pile, the computed maximum lateral deformations are 17.8 mm and 19 mm for the double-paddled and single-paddled piles with $L_p = 550$ mm, respectively. Generally, as the plate length increases, there is a corresponding decrease in lateral displacement. However, the increase in lateral capacity becomes negligible for single-paddled piles with $L/W_p \geq 3.5$ and for double-paddled piles with $L/W_p \geq 4.5$. The disparity in lateral capacity between double- and single-paddled piles is insignificant for $L/W_p \leq 1.5$ and escalates as this ratio increases. At $L/W_p = 3.5$, the calculated difference in lateral displacement is approximately 5 mm; as L/W_p continues to rise, the impact of adding a second plate remains constant. Stiffness efficiency analyses were conducted across various L/W_p values to ascertain the percentage increase in capacity for design optimization. Double- and single-paddled piles with a plate length of 0.25 L (550 mm) exhibit higher capacity than the plain pile by 21% and 16%, respectively, as depicted in Figure 17. It is expected that η_s increases with L. For a plate length of 2325 mm, the stiffness efficiency rises by 341% and 119% for double- and single-paddled piles, respectively. In the studied configuration, the increase in stiffness efficiency becomes negligible for $L/W_p \geq 4$ for both single- and double-paddled piles.

The effect of plate length for double-paddled piles was also investigated considering a system with identical lengths for the pile and plate. The results indicate significantly higher lateral displacement (64.1 mm) than the first system (6.2 mm), for the pile with a length of 1.74 m. Nevertheless, a sufficient lateral capacity was obtained for an embedded pile-plate length of 2.20 m with $L/W_p = 4.7$, and with approximately 1 mm less than the recorded value for the 3.5 m long pile. The effect of increasing the pile length becomes negligible as L/W_p increases.

The lateral displacement profiles for both examined systems are presented in Figures 18 and 19. In a system where plates are welded to an H-pile with a fixed embedded length of 3.5 m, the observed behavior aligns with that of a flexible pile. Conversely, the behavior resembling that of a short pile becomes apparent in a system where the plate-pile length is identical and the ratio of length to plate width (L/W_p) is ≤ 6 . Piles with a ratio of length to plate width (L/W_p) ≥ 7 demonstrate the behavior of a fixed pile. The results further suggest that the depth at which fixation occurs, marked by zero lateral deflection and slope, is approximately -2.8 m (equivalent to 5 to 6 W_p). As a result, the soil characteristics within the top 5 to 6 W_p significantly impact the lateral behavior of the proposed H-pile. These results are consistent with those reported by Abouzaid and El Naggar [18] for PHPs in clay soil. Thus, there exists an optimal range of plate width that balances the load-bearing capacity of the post with the width ratio, ensuring an efficient design for the innovative post. These outcomes provide valuable insights for optimizing the design of innovative posts in engineering applications.

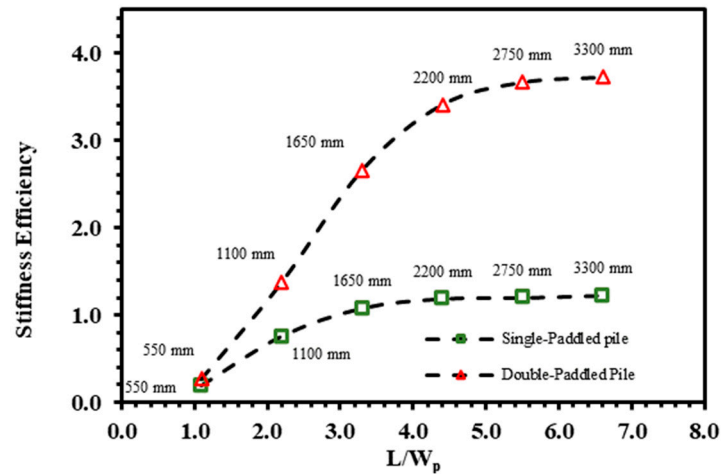


Figure 17. Stiffness efficiency for various L/W_p values.

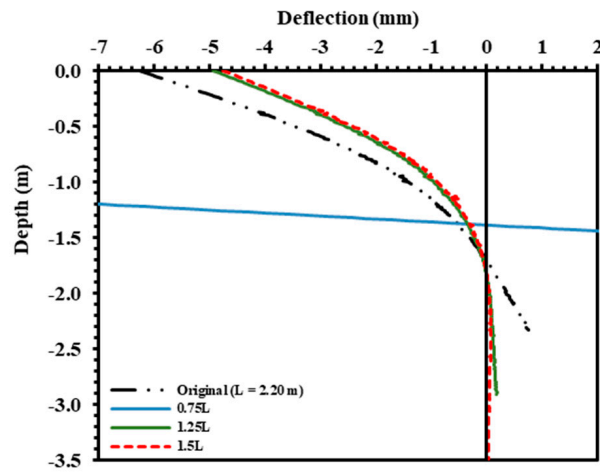


Figure 18. Lateral deflection profile for double-paddled piles, with $L_p = 3.5$ m, $W_p = 500$ mm, and $L/W_p = 1.2, 2.3, 3.5, 4.7, 5.8, 7.0$.

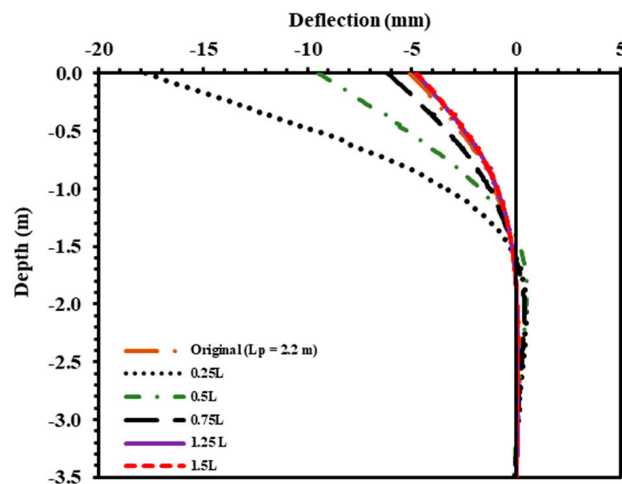


Figure 19. Lateral deflection profile for double-paddled piles ($W_p = 500$ mm, and varying L/W_p ratio).

6.4. Performance of Clipped-Paddled Posts vs. Welded-Paddled Posts

In this section, the effectiveness of two manufacturing techniques for innovative posts (IPs) is examined: welded plate (WS20) and clipped plates (CS20). It is anticipated that WS20 would exhibit a higher lateral load capacity due to the additional stiffness and

resistance resulting from the increased cross-sectional area and a slight increase in the moment of inertia. The horizontal load-displacement responses of the clipped plate piles (CDP and CSP) and their corresponding welded plate piles are depicted in Figure 20.

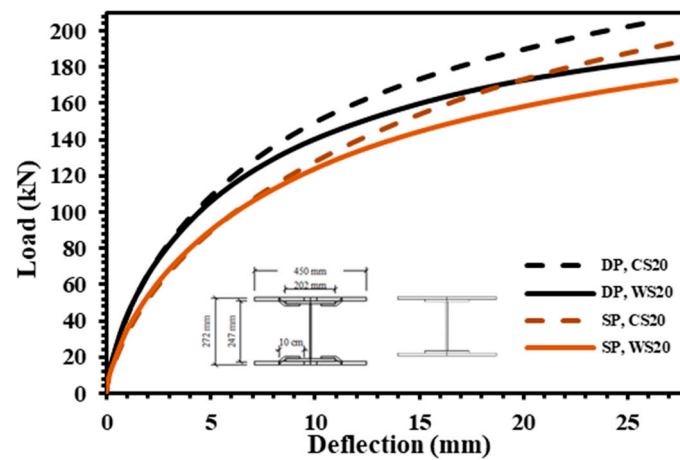


Figure 20. Comparison of load-displacement curves considering different manufacturing methods.

The findings based on New York City [32] specifications indicate that clipping the plates enhances the capacity of IP by approximately 12% and 8% for DP and SP, respectively. Notably, an exact match is observed between the clipped plates and the corresponding welded plates for the initial 6 mm of lateral displacement. This suggests that the clipped plates provide comparable performance to the welded plates during the early stages of lateral displacement.

6.5. Effect of Plates on Surrounding Soil

The capacity of piles subjected to lateral loads is controlled by the rigidity of the pile, as well as the stiffness and strength of the surrounding soil. It is assumed that the influence zone of a laterally loaded pile takes the form of a three-dimensional inverted cone near the ground surface, centered on the pile [43]. The key factor affecting the lateral resistance of the pile is the deformation of the soil within this influence zone [41]. Consequently, this analysis focuses on evaluating the interaction between paddled piles and the soil within the zone of influence.

Figure 21 displays the typical patterns of lateral displacement for the pile and surrounding soil due to a lateral load applied at the pile head. The extent of the influence zone for different plate widths is shown in Table 7. It is observed that the size of influence zone increases significantly as the plate width increases, ranging from 1.9 m to 2.7 m along the load direction (Y-direction) and from 1.0 m to 1.7 m perpendicular to load direction (X-direction).

Table 7. Extent of soil influence around double-paddled piles.

W _p (mm)	Disturbed Zone (m)	
	Y-Direction	X-Direction
250	1.88	1.03
375	2.36	1.31
500	2.37	1.33
625	2.4	1.42
750	2.62	1.60
875	2.64	1.62
1000	2.67	1.64
1125	2.67	1.66

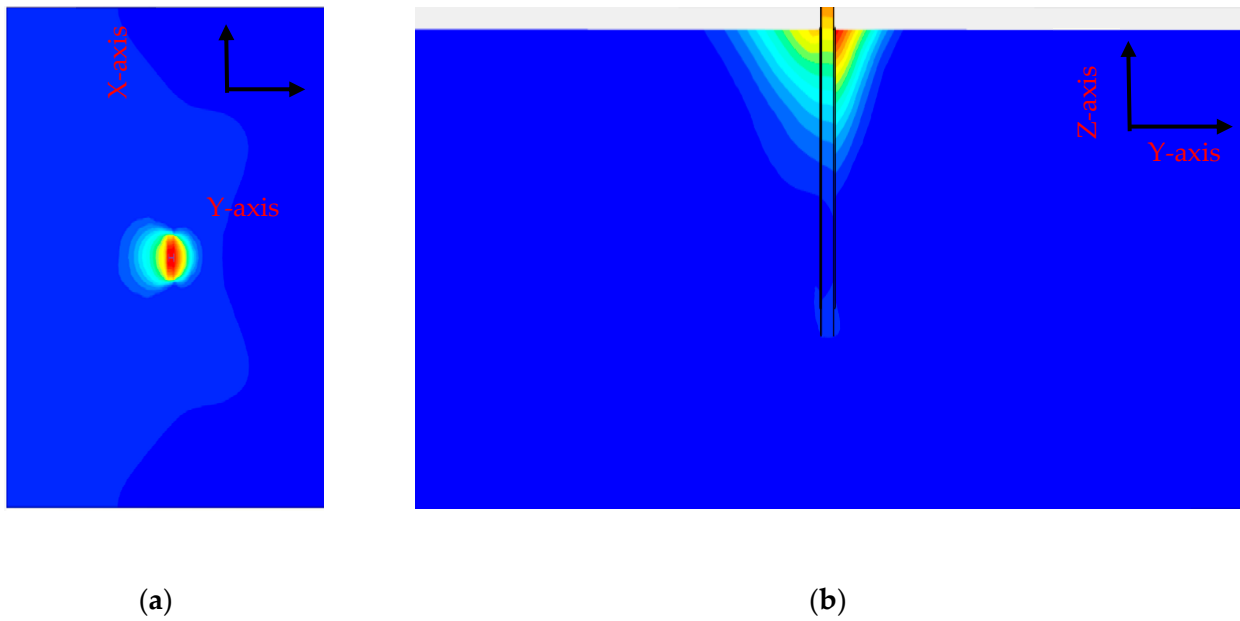


Figure 21. Typical total lateral displacement (U_y) behavior of soil and pile under lateral load: (a) horizontal cross-section; (b) vertical cross-section.

Figure 22 presents the variation of influence zone factor with the plate width. The influence zone factor is defined as the extent of influence zone normalized by the plate width for both horizontal directions. The influence zone extends from $2.4 W_p$ and $1.5 W_p$ to $7.5 W_p$ and $4.1 W_p$ for X and Y directions, respectively.

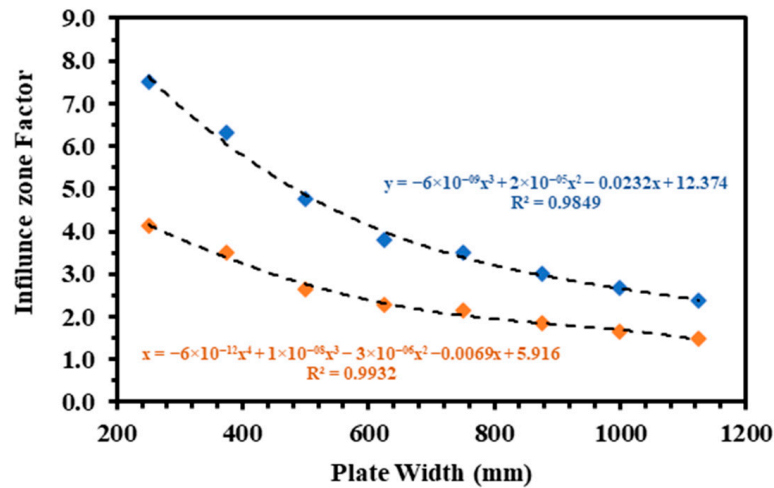


Figure 22. Influence zone factor (influence distance/plate width) considering different plate widths.

The data were curve fitted and the following equations can be obtained:

$$Y (m) = -6 \times 10^{-9} W_p^3 + 2 \times 10^{-5} W_p^2 - 0.0232 W_p + 12.374$$

$$X (m) = -6 \times 10^{-12} W_p^4 + 1 \times 10^{-8} W_p^3 - 3 \times 10^{-6} W_p^2 - 0.0069 W_p + 5.916$$

where Y , X , and W_p are the influence zone along the load direction, perpendicular to the load direction, and width of the plate, respectively.

Illustrating the behavior of both the pile and soil, Figure 23 displays iso-surface plots of phase shear strain $P\gamma_s$, highlighting the scope of the soil influence zone at various W_p/W_f values based on the original S16 dimensions. The introduction of plates to the flanges of the H-pile results in a reduction of shear strain development in the loading direction when

compared to the traditional H-pile. This impact becomes less pronounced as WP increases (e.g., $W_p/W_f = 750$). With a small plate width (e.g., $W_p/W_f = 250$), the soil influence zone mobilizes rapidly, encompassing the entire plate width, involving the entire paddle in soil resistance mobilization. Conversely, for W_p/W_f values of 650 or higher, the development of the mobilized soil influence zone is slower, and the contribution of the plate to lateral load resistance becomes insignificant. As a result, part of the plate is excluded from the mobilized influence zone.

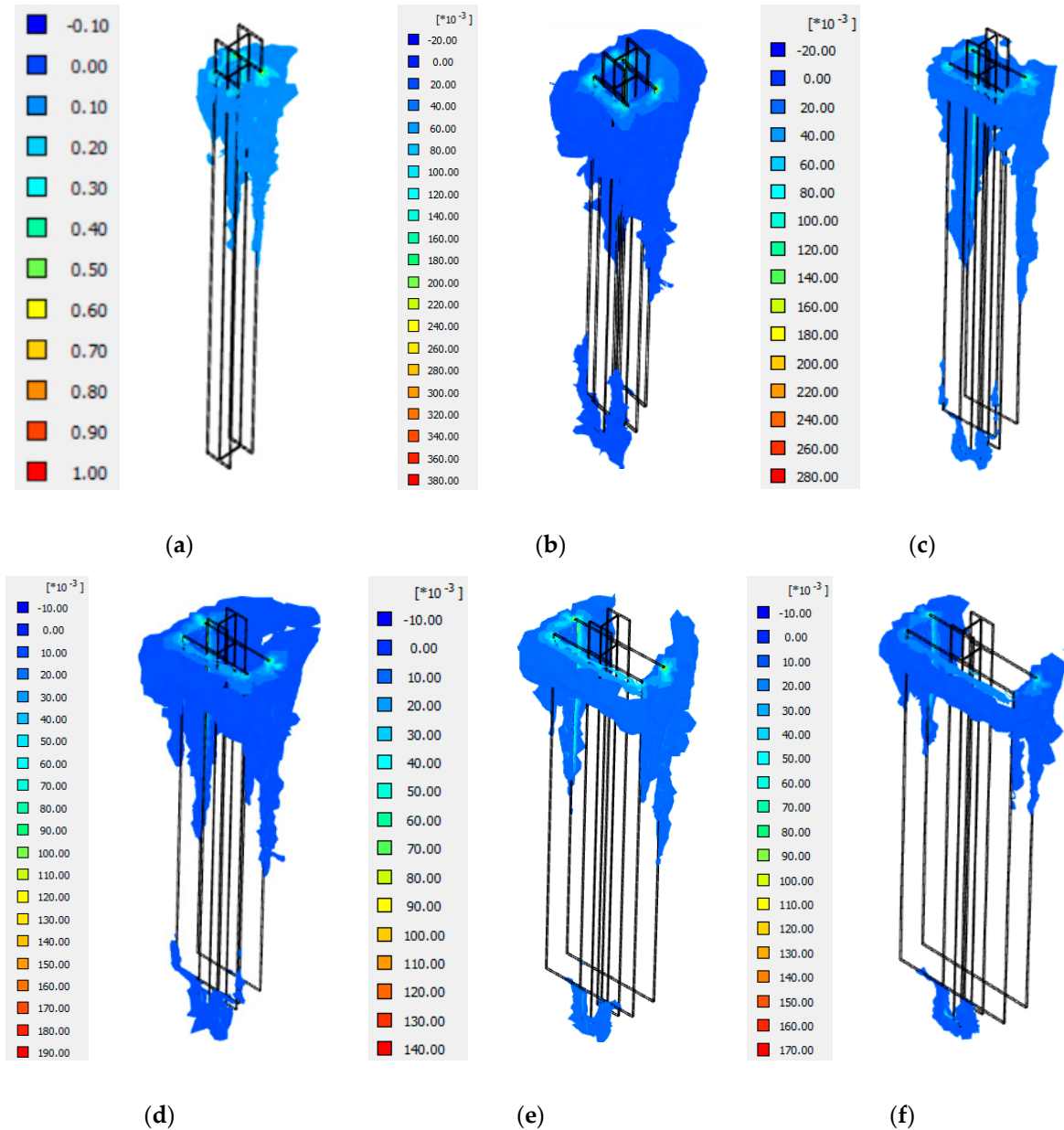


Figure 23. Comparison of phase shear strain on plain piles and double-paddled piles at different W_p/W_f values: (a) plain pile; (b) $W_p/W_f = 250$; (c) $W_p/W_f = 375$; (d) $W_p/W_f = 500$; (e) $W_p/W_f = 625$; (f) $W_p/W_f = 750$.

7. Conclusions

This study assessed the efficacy of newly proposed structural supports designed for lateral loads. This innovative foundation system comprises one or two plates attached to the flanges of a steel H-pile. Using 3D FEMs developed in PLAXIS 3D software, the lateral behavior of both single- and double-paddled piles, installed in sandy soil, was simulated.

Comparing the numerical predictions and field load test results revealed good agreement, confirming the ability of the developed numerical models to accurately replicate the lateral response of the innovative supports. Utilizing these validated models, we conducted further analyses on the response of the innovative post were analyzed considering various configurations, leading to the following conclusions: Stiffening the H-pile with plates significantly increases the lateral capacity of the foundation. The calculated load-carrying efficiency varies between 57% to 83% for double-paddled piles and 35% to 63% for single-paddled piles.

1. The lateral displacement capacity of the single-paddled pile is 30% to 55% less than that of the double-paddled pile (5 mm less than the double-paddled H-pile). However, its cost is anticipated to be less than the double-paddled pile.
2. Stiffness efficiency of the innovative post is realized for $W_p/W_f < 4$ or $L/W_p < 4.5$ in a double-paddled pile system and $W_p/W_f < 3$ or $L/W_p < 3.5$ in a single-paddled pile system.
3. The plate width has a greater effect on the lateral capacity of the innovative post than plate length.
4. Adding plates reduce the maximum bending moment along the pile shaft, as well as the bending moment profile along the pile, especially for larger W_p .
5. The soil along the top 5–6 W_p of the pile govern the lateral response of the proposed post.
6. Based on stiffness efficiency, an optimal paddle width of $W_p/W_f = 4$ and 3 is identified for double- and single-paddle piles, respectively. The optimal paddle length is suggested to be $L/W_p \geq 4.5$ for the plate width considered in the present study.

For a comprehensive understanding of how paddled H-piles behave when supporting laterally loaded structures such, it is advisable for future research to study the dynamic behavior of the proposed foundation system caused by wind loads. Employing the hardening soil model for dynamic analysis is also recommended. Furthermore, exploring the effects of combined load conditions, encompassing both vertical and lateral loads on paddled H-piles, would offer valuable insights into the overall system performance. Lastly, investigating the impact of vibratory driving of the PHPs on the soil through field and laboratory tests is recommended.

Author Contributions: A.A.: Conceptualization, data curation, formal analysis, investigation, methodology, software, validation, visualization, writing original draft, writing review and editing. M.H.E.N.: Conceptualization, funding acquisition, project administration, resources, methodology, supervision, writing review and editing. O.D.: software, writing review and editing. All authors have read and agreed to the published version of the manuscript.

Funding: I would like to thank Mitacs Accelerate Program. This research was for funded by Mitacs Accelerate, grant number IT29511.

Institutional Review Board Statement: Not applicable.

Informed Consent Statement: Not applicable.

Data Availability Statement: The data presented in this study are available on request from the corresponding author.

Acknowledgments: I would like to acknowledge Atlantic Industries Limited, particularly Dereck Essery, for their support and constructive feedback on this work. Additionally, I am grateful to Mitacs for their support through the Mitacs Accelerate Program.

Conflicts of Interest: The authors declare no conflicts of interest.

References

1. Long, J.H.; Vanneste, G. Effects of Cyclic Lateral Loads on Piles in Sand. *J. Geotech. Eng.* **1994**, *120*, 225–244. [[CrossRef](#)]
2. Basack, S.; Nimbalkar, S. Measured and Predicted Response of Pile Groups in Soft Clay Subjected to Cyclic Lateral Loading. *Int. J. Géoméch.* **2018**, *18*, 04018073. [[CrossRef](#)]
3. Matlock, H.; Reese, L.C. Generalized Solutions for Laterally Loaded Piles. *J. Soil Mech. Found. Div.* **1960**, *86*, 63–92. [[CrossRef](#)]

4. Davisson, M.T. *Behavior of Flexible Vertical Piles Subjected to Moment, Shear, and Axial Load*; University of Illinois: Champaign, IL, USA, 1960.
5. Broms, B.B. Lateral Resistance of Piles in Cohesionless Soils. *J. Soil Mech. Found. Div.* **1964**, *90*, 123–156. [[CrossRef](#)]
6. Matlock, H. Correlation for Design of Laterally Loaded Piles in Soft Clay. In Proceedings of the 2nd Offshore Technology Conference, Houston, TX, USA, 22–24 April 1970; pp. 577–594. [[CrossRef](#)]
7. Reese, L.C.; Cox, W.R.; Koop, F.D. Analysis of laterally loaded piles in sand. In Proceedings of the Offshore Technology Conference, Houston, TX, USA, 5–7 May 1974; University of Houston: Houston, TX, USA, 1974; pp. 95–105. [[CrossRef](#)]
8. Winkler, E. *The Teaching of Elasticity and Strength with Special Regard to Their Application in Technology for Polytechnic Schools, Construction Academies, Engineers, Mechanical Engineers, Architects*; Dominicus, H., Ed.; Dominicus: Prague, Czech Republic, 1867.
9. El Naggar, M.H.; Wei, J.Q. Response of tapered piles subjected to lateral loading. *Can. Geotech. J.* **2011**, *36*, 52–71. [[CrossRef](#)]
10. Peng, J.; Clarke, B.G.; Rouainia, M. Increasing the Resistance of Piles Subject to Cyclic Lateral Loading. *J. Geotech. Geoenvironmental Eng.* **2011**, *137*, 977–982. [[CrossRef](#)]
11. Grabe, J.; Dührkop, J. Improving of lateral bearing capacity of mono-piles by welded wings. In *Proceedings of the 2nd International Conference on Foundations*; HIS BRE Press: Garston, UK, 2007.
12. Peng, J.-R.; Rouainia, M.; Clarke, B. Finite element analysis of laterally loaded fin piles. *Comput. Struct.* **2010**, *88*, 1239–1247. [[CrossRef](#)]
13. Mroz, D.; El Naggar, M.H.; Director, R.; El Sharnouby, M.; Essery, D. Experimental and Numerical Evaluation of Plate Modified H-Piles Subjected to Monotonic and Cyclic Lateral Loading. In Proceedings of the TAC Conference & Exhibition, Ottawa, ON, Canada, 8 October–21 September 2020.
14. Dührkap, J.; Grabe, J. Laterally loaded piles with bulge. *J. Offshore Mech. Arct. Eng.* **2008**, *130*, 041602. [[CrossRef](#)]
15. Lutenegger, A.J. Tension Tests on Driven Fin Piles for Support of Solar Panel Arrays. In Proceedings of the GeoCongress 2012: State of the Art and Practice in Geotechnical Engineering, Oakland, CA, USA, 25–29 March 2012; pp. 305–314. [[CrossRef](#)]
16. Abongo, K.O. Model Study of the Static and Cyclic Lateral Capacity of Finned Piles. 2019. Available online: <https://preserve.lehigh.edu/etd/4336> (accessed on 21 December 2023).
17. Pei, T.; Qiu, T. A Numerical Investigation of Laterally Loaded Steel Fin Pile Foundation in Sand. *Int. J. Géoméch.* **2022**, *22*, 04022102. [[CrossRef](#)]
18. Abouziad, A.; El Naggar, M.H. Experimental and Numerical Analysis of Laterally Loaded Single- and Double-Paddled H-Piles in Clay. *Geotechnics* **2023**, *3*, 1324–1345. [[CrossRef](#)]
19. Mroz, D. Experimental and Numerical Evaluation of a Novel Piling System for Sound Wall Applications. Ph.D. Thesis, The University of Western Ontario, London, ON, Canada, 2019. Available online: <https://ir.lib.uwo.ca/etd/6563> (accessed on 24 November 2023).
20. Kézdi, Á.; Rétháti, L. *Handbook of Soil Mechanics*; Elsevier: Amsterdam, The Netherlands, 1974; Volume 1.
21. Bowles, J.E. *Foundation Analysis and Design*, 5th ed.; St. Louis San Francisco: Springfield, MO, USA; The McGraw-Hill Companies, Inc.: New York, NY, USA, 1996.
22. Kumar, R.; Bhargava, K.; Choudhury, D. Estimation of Engineering Properties of Soils from Field SPT Using Random Number Generation. *INAE Lett.* **2016**, *1*, 77–84. [[CrossRef](#)]
23. Kulhawy, F.H.; Chen, J.-R. Discussion of ‘Drilled Shaft Side Friction in Gravelly Soils’ by Kyle M. Rollins, Robert J. Clayton, Rodney C. Mikesell, and Bradford C. Blaise. *J. Geotech. Geoenviron. Eng.* **2007**, *133*, 1325–1328. [[CrossRef](#)]
24. *ASTM D3966-07*; Standard Test Methods for Deep Foundations Under Lateral Load. ASTM Standards: West Conshohocken, PA, USA, 2010. [[CrossRef](#)]
25. McAulity, J.F.M. Thrust Loading on Piles. *J. Soil Mech. Found. Div.* **1956**, *82*, 1–25. [[CrossRef](#)]
26. Cox, J.N.W.A.E.H. Design of Pier Foundations for Lateral Loads. *Trans. ASAE* **1966**, *9*, 417–420. [[CrossRef](#)]
27. Drbe, O.; El Naggar, H. Investigation of Hollow Bar Micropiles in Cohesive Soil. 2013. Available online: <https://ir.lib.uwo.ca/etdhttps://ir.lib.uwo.ca/etd/1770> (accessed on 21 December 2023).
28. Guo, P.; Xiao, Y.; Kunnath, S. Performance of laterally loaded H-piles in sand. *Soil Dyn. Earthq. Eng.* **2014**, *67*, 316–325. [[CrossRef](#)]
29. Tomlinson, M.; Woodward, J. *Pile Design and Construction Practice*, 6th ed.; CRC Press: Boca Raton, FL, USA, 2015; pp. 1–575. [[CrossRef](#)]
30. Kasch, V.R.; Coyle, H.; Bartoskewitz, R.E.; Sarver, W.G. Lateral Load Test of a Drilled Shaft in Clay. 1977. Available online: <https://onlinepubs.trb.org/Onlinepubs/trr/1979/733/733-007.pdf> (accessed on 21 December 2023).
31. Poulos, H.; Davis, E. *Pile Foundation Analysis and Design*; Wiley: New York, NY, USA, 1980.
32. *Building Code of the City of New York*; Gould Publications: Binghamton, NY, USA. Available online: <https://www.nyc.gov/site/buildings/codes/nyc-code.page> (accessed on 23 November 2023).
33. Kim, Y.; Jeong, S. Analysis of soil resistance on laterally loaded piles based on 3D soil–pile interaction. *Comput. Geotech.* **2011**, *38*, 248–257. [[CrossRef](#)]
34. Nusairat, J.; Liang, R.Y.; Engel, R.; Hanneman, D.; Abu-Hejleh, N.; Yang, K. Drilled Shaft Design for Sound Barrier Walls, Signs, and Signals. 2004. Available online: <https://www.codot.gov/programs/research/pdfs/2004/drilledshaft.pdf> (accessed on 21 December 2023).
35. Sheil, B.B.; McCabe, B.A. Predictions of friction pile group response using embedded piles in PLAXIS. In Proceedings of the 3rd International Conference on New Developments in Soil Mechanics and Geotechnical Engineering, Nicosia, Cyprus, 28 June 2012.

36. Al-Abboodi, I.; Sabbagh, T.T. Numerical Modelling of Passively Loaded Pile Groups. *Geotech. Geol. Eng.* **2019**, *37*, 2747–2761. [[CrossRef](#)]
37. PLAXIS CONNECT Edition V22.01 PLAXIS 3D-Reference Manual. 2022. Available online: https://communities.bentley.com/cfs-file/_key/communityserver-wikis-components-files/00-00-00-05-58/PLAXIS_5F00_3D_5F00_CEV22.01_5F00_2_2D00_Reference.pdf (accessed on 21 December 2023).
38. Chik, Z.; Abbas, J.M.; Taha, M.; Shafiqu, Q.S. Lateral behavior of single pile in cohesionless soil subjected to both vertical and horizontal loads. *Eur. J. Sci. Res.* **2009**, *29*, 194–205.
39. Deendayal, R.; Muthukkumaran, K.; Sitharam, T.G. Response of laterally loaded pile in soft clay on sloping ground. *Int. J. Geotech. Eng.* **2016**, *10*, 10–22. [[CrossRef](#)]
40. Rafea, O.; Andrzej, T. The Hardening Soil Model-A Practical Guidebook. 2018. Available online: <http://www.zsoil.com> (accessed on 21 December 2023).
41. Nasr, A.M. Experimental and theoretical studies of laterally loaded finned piles in sand. *Can. Geotech. J.* **2013**, *51*, 381–393. [[CrossRef](#)]
42. Babu, K.V.; Viswanadham, B.V.S. Numerical studies on lateral load response of fin piles. *Géoméch. Geoengin.* **2019**, *14*, 85–98. [[CrossRef](#)]
43. Murff, J.D.; Hamilton, J.M.; Murff, M.J.D.; Member, A. P-Ultimate for Undrained Analysis of Laterally Loaded Piles. *J. Geotech. Eng.* **1993**, *119*, 91–107. [[CrossRef](#)]

Disclaimer/Publisher’s Note: The statements, opinions and data contained in all publications are solely those of the individual author(s) and contributor(s) and not of MDPI and/or the editor(s). MDPI and/or the editor(s) disclaim responsibility for any injury to people or property resulting from any ideas, methods, instructions or products referred to in the content.